Wind Tunnel Experiment of UTM-SACCON UCAV Configuration

Khushairi Amri Kasim[1*], Shabudin Mat[1], Shuhaimi Mansor[1]

[1]School of Mechanical Engineering, Faculty of Engineering, Universiti Teknologi Malaysia, 81310 UTM Skudai, Johor, Malaysia

Corresponding author* email: shabudin@utm.my
Available online 20 June 2022

ABSTRACT

The rapid development and advancement in unmanned aerial vehicle/unmanned combat aerial vehicle (UAV/UCAV) has triggered the increasing interest in development of UAV/UCAV. Numerous of the research performed experimentally and numerically in order to have a better understanding on the complicated flow behavior above low sweep blended delta wing design which commonly used in UCAV configuration. A research group called AVT-161 is one of the pioneer research programmes in the UCAV configuration throughout generic model SACCON. However, the current knowledge on the SACCON configuration is very limited to certain angle of attacks and flow conditions such Reynold number. This current research will highlight the aerodynamics and flow characteristics of the SACCON at Reynolds number of 0.51×10^6 and 0.78×10^6 towards different angle of attacks. A semi-span wind tunnel model was designed and fabricated with the capability to install pressure taps on several positions inside the model. The experiments were conducted in a closed-circuit low speed wind tunnel at speeds of 17 and 26 m/s that corresponding to 0.51×10^6 and 0.78×10^6 Reynolds numbers based on model mean aerodynamic chord, respectively. The angles of attack were varied from -10° to 30°. During the experiment, two measurement techniques were employed on the wing, which were the steady balance measurement and surface pressure measurement. The findings highlight the effects of Reynolds number toward the aerodynamic coefficients and pressure distribution above the wing. The experimental data conclude that the aerodynamic characteristics of SACCON wing is influenced by flow structure above the wing. The SACCON wing exhibits three major vortex structures which are apex vortex, thickness vortex and tip vortex. Additional suction peak is observed near the trailing edge downstream from wing at higher angle of may suggest that another vortex developed in the region. The current findings may contribute to a better understanding of flow physics on UCAV configuration.

Keywords: wind tunnel experiment, SACCON configuration, vortex, delta wing, lambda wing, UCAV

1. Introduction

Throughout the years, there have been rapid development on the unmanned aerial vehicle/unmanned combat aerial vehicle (UAV/UCAV) around the world due their prevalent applications in civil and military sectors [1]. UAV/UCAV or unmanned aircraft is an air vehicle without pilot onboard and can be remotely controlled or autonomously. This development had raised the improvement in wide scale application regarding unmanned aircraft such in monitoring, surveying, inspection and emergency response [2]. Considering the flexibility in operation and wide area coverage, unmanned aircraft is more favourable compared to the ground approaches [3]. Aside from high mobility, the employment of unmanned aircraft also reduces the operational cost as well as prevent any casualties toward the operators [4-6]. For UCAV, their function is not limited only to reconnaissance, surveillance and intelligence mission. UCAV commonly equipped with aircraft ordnance such bombs, missiles and rockets for airstrike mission [7].

The advancement of the technology has triggered essential of UCAV that capable of higher speed and manoeuvre alongside with specific mission requirement. Thus, delta wing concept was introduced in UCAV development to achieve required conditions. Most of the current and future UAV/UCAV configurations are using delta wing planform with low to medium sweep angle i.e., 35° to 55° [8][9]. This is due to the considerations of the performance and endurance of the real flight [10]. The delta wing design is having aerodynamic advantages and higher power efficiency compared to the conventional wing which enable operation at near and post stall regimes for extra aerodynamic lift. The extra lift generated from the leading-edge vortex improve overall lift generation on the wing and beneficial at lower angles of

attack condition [11]. The most common planform used in current and future delta-winged UCAV are diamond and lambda wing as shown in Figure 1. The lambda wing planform features a cranked design at the trailing edge meanwhile diamond wing incorporated extended trapezoidal trailing edge. The delta-winged UCAV design commonly incorporated blended wing design to produce higher volume for larger payloads and system/equipment integrations. The blended wing design introduce inconsistent leading-edge radius from the apex of the wing toward trailing edge which induced complicated vortical flow above the wing. The attached flow region near the apex will influenced the formation of leading-edge vortex downstream depending on the flow conditions i.e., angle of attack, Reynolds number and leading-edge profile [12].

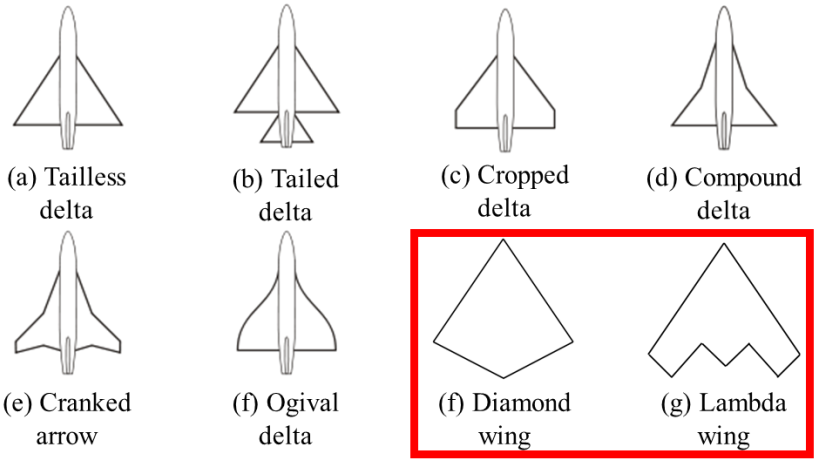

Figure. 1. Types of delta wing used in aircraft and UAV/UCAV

Throughout the world, numerous manufacturers are working and developing UCAV design configuration for current and future uses. There are several aircraft UCAVs available and are operating as shown in Figure 2. Most of the UCAV design incorporated with the lambda wing planform with highly blended wing design. This is mainly due to the stealth requirements priority [13]. Air forces and defence companies are currently investing in long term development of sixth-generation fighter aircraft to be employed in service by year of 2035-2040 [14]. The sixth-generation fighter aircraft will be incorporated with the unmanned features. Several such ongoing projects are BAE Systems Tempest (Europe), F/A-XX (United States) and Mikoyan PAK DP (Russia). However, to develop the agile and highly swept UCAV configuration is very demanding endeavour. The essential performance and manoeuvrability requirement from the UCAV design required tremendous, detailed data such aerodynamic performance at extensive flight conditions, mass distribution, system integration and propulsion performance [15]. At times, the UCAV design and development is compromised between high-speed flight performance and manoeuvrability at low-speed flight [16].

Figure. 2. Current and future UCAV design used in aircraft

Due to rapid advancement in UCAV development, there has been increasing interest in understanding the flow characteristics on non-slender delta wing used in UCAV configurations. Numerous of studies were performed to understand the flow behaviour around the low sweep blended delta wings through the experiments and to provide validation data for evaluation of the major CFD codes. The first program on UCAV configuration was organised by The Technical Cooperation Program (TTCP). The program was focussing on the 1303 UCAV configuration. Another research group then established their UCAV configuration program under applied vehicle technology (AVT-161) entitled "Assessment of Stability and Control Prediction Methods for NATO Air & Sea Vehicles".

2. SACCON UCAV Configuration

AVT-161 research group programme was established to determine capability of computational methods for predicting the stability of modern aircraft concerning vortex dominated flow field. The task group consist of three major sections namely, experimental, computational fluid dynamic (CFD) and stability and control. This task group is a continuation from previous AVT program AVT-080 and AVT-131. A generic UCAV model called SACCON (Stability And Control CONfiguration) was developed [17]. The SACCON configuration was developed to have The SACCON configuration was designed to have clearer view on many aspects of UCAV concepts and at the same time being suitable for international collaborative research [18]. The SACCON model has a lambda planform with leading edge sweep of 53°. The wing was designed with approximately 1 metre root chord and 1.54 metre wingspan length. This model was designed specifically to generate complex vortices interaction above the wing resulting in non-linear aerodynamic characteristic [15]. The model consists of three main parts which are fuselage, wing section and wing tip. Three different profiles were used at each part. The different profile at root of fuselage and wing section generated blended transition wing. Then outer wing section is having 5° twist angle around the leading edge. This configuration produced inconsistent leading-edge radius along the wing chord. The detailed model specification and dimension is available in [16]. The information on the profiles used in designing SACCON model is limited by the lack of information due to classified information within the research group.

To date, there are five SACCON models built for wind tunnel testing. The first original model was built during the AVT-161 Task Group which focussing on aerodynamic stability and control with detailed flow physics for the clean configuration wing [19]. Four another wind tunnel model was built to conduct experiments in AVT-201 programme [20]. During AVT-201 program, the original SACCON was modified by adding control devices on the left side of the wing and named DLR F-17 model. Later, DLR F-19 model was built based on the SACCON geometry with control devices on both wing sides. This includes extra control devices on both side of the wing tips. The DLR F-17E was designed for high-speed flow conditions up to the transonic speed. This model also was built with trailing edge control devices same as DLR F-17 and DLR-F19 configurations. Last model was built within the AVT-201 was ONERA SACCON with clean configuration to extend the dynamic experimental data. First semi-span SACCON wind tunnel model was built at University of Arizona (UA) with clean configuration [21]. The details on the existing SACCON wind tunnel are summarised in Table 1.

The current research highlights the current experiments on generic UCAV configuration named SACCON at lower Reynolds number and various angle of attack. To date, there are limited information available on aerodynamic characteristics and flow behaviour above this wing especially at low Reynolds number range.

Table 1. Existing wind tunnel SACCON model

Wind Tunnel Model	Size and Configuration	Test Facility
Original SACCON (AVT-161)	Full span model; cr =1.0608m, s=0.769m; Clean configuration without control surfaces	DNW-NWB NASA LaRC
DLR F17 (AVT-201)	Full span model; cr =1.0608m, s=0.769m; With control surfaces on the left wing (modified from original SACCON)	DNW-NWB
DLR F19 (AVT-201)	Full span model; cr =1.0608m, s=0.769m; With control surfaces on both sides of wing	DNW-NWB
DLR F17E (AVT-201)	Full span model; cr =0.414m, s=0.3m; With control surfaces	DNW-TWG HSWT
ONERA SACCON (AVT-201)	Full span model; cr =0.6897m, s =0.5m; Clean configuration without control surfaces	ONERA SV4 & L1
UA SACCON	Semi span model; cr =0.743, s =0.538m; Clean configuration without control surfaces	UA Aerolab

3. UTM SACCON MODEL

A semi-span model was designed and fabricated in UTM Aerolab that replicate the original SACCON from AVT-161. The design and dimension of the model is based on the model used within AVT-161 programme. The model was designed to have semi-span model to accommodate the availability test section size without compromising the model dimension. The stand-off for the model was designed based on the fuselage profile and dimension. Figure 3 shows the UTM-SACCON wind tunnel model specification and dimension. To measure the pressure on the upper surface of the wing, the model has been installed with 99 pressure taps with diameter of 1 mm located on the entire wing. The pressure taps are connected to the pressure scanner through the vinyl tube.

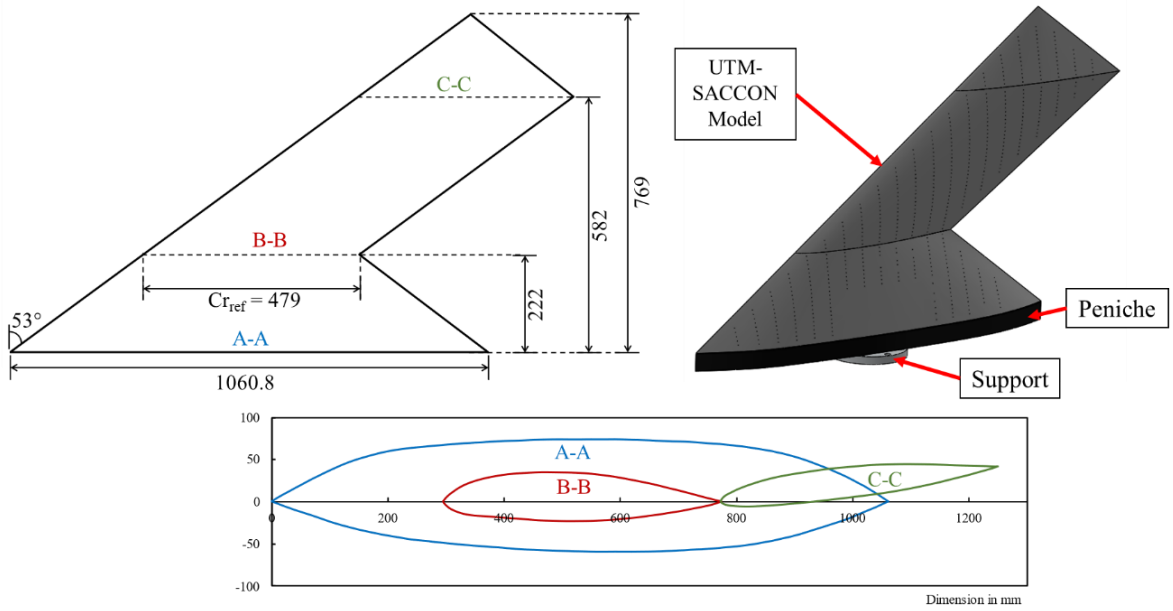

Figure. 3. UTM-SACCON configuration dimension and geometrical properties

The experiments were performed in the UTM Aerolab wind tunnel. The size of the test section is 2m x 1.5m x 5m with the capability of 80 m/s maximum speed. The installation of the model in the test section is shown in Figure 4 with notation of forces and moments. Fx, Fy and Fz represent the direction of drag, lift and side force of the model while Mz represent the model pitching moment. The model is attached to 6-component external balance JR3 160M50 located underneath the test section. The UTM-SACCON wind tunnel model was mounted above additional stand-off (*peniche*) to avoid the flow interactions between wind tunnel boundary layer with the model.

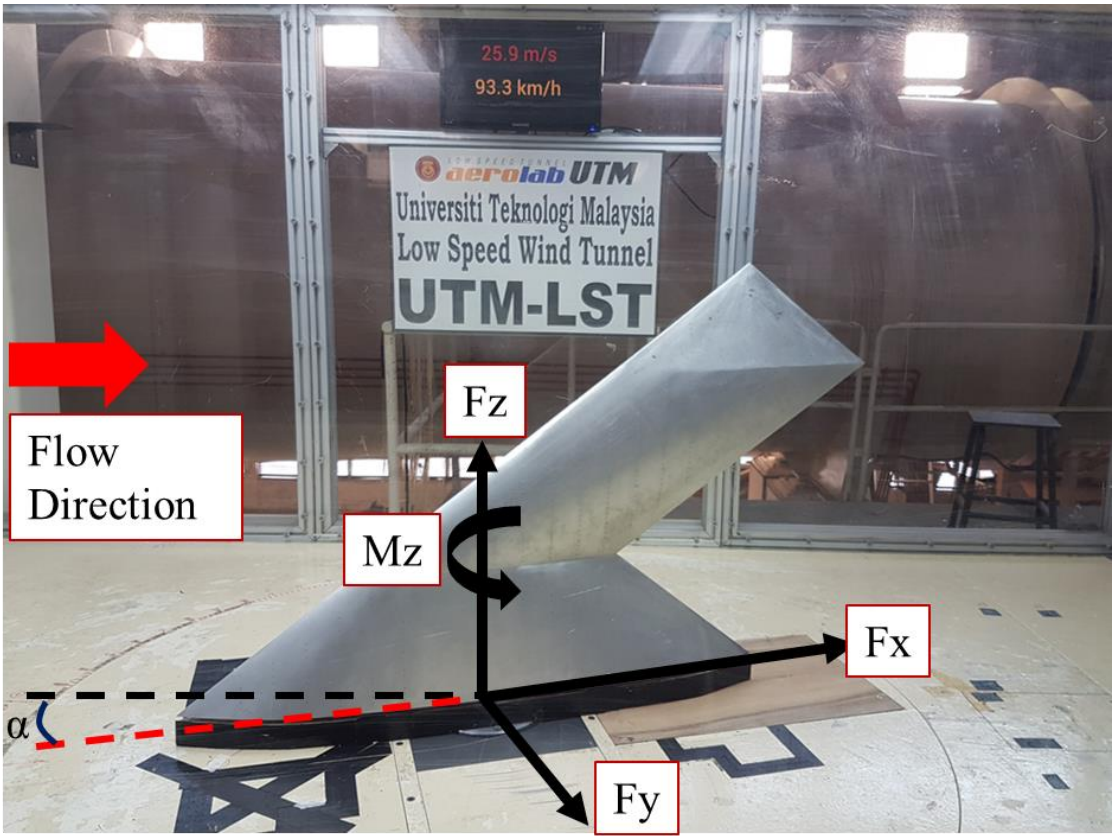

Figure. 4. Installation of UTM-SACCON with forces and moment notation

The experiments were performed at the speeds of 17 and 26 m/s that corresponding to 0.51×10^6 and 0.78×10^6 Reynolds number based on reference chord of 0.479 meter. The angles of attack were varied from -10° to 30° by controlling the wind tunnel turntable automatically. In this study, two measurement techniques were employed on the wing. The first measurement technique was the steady balance data while the final one was the surface pressures measurement. All forces and moments in x, y and z have been recorded at three times sampling and repeatability process had been considered. The measured force in the y and x directions were normalized into the lift and drag coefficients (C_L & C_D) of the model while the moment in z direction is converted into the wing pitching moment coefficient (C_M). The uncertainty analysis was performed for all forces and moments channel. The standard error was then calculated separately for these forces and moments channel at each angle of attack. The maximum uncertainty of data for all forces and moments channel is at 0.6%. The pressure measurement on the surface was obtained at measurement planes of 0.1 to 0.9. The pressure distribution on plane 0.4 to 0.6 is limited in the fuselage section is due to restriction in the model cavity (placement of the wing support to the tunnel). The surface pressure measurement was recorded using the FKPS 30DP electronic pressure scanner with an accuracy of ±1 psi. The measured pressures then were converted into pressure coefficients (C_P). Only selected angle of attack for pressure distribution above the wing is presented within this paper. Table 2 shows the experiment conditions in this paper.

Table 2. Experiment conditions

Parameters	Values
Pressure distribution measurement planes (Y/Cr)	0.1, 0.2, 0.3, 0.4, 0.5, 0.6, 0.7, 0.8, 0.9
Freestream velocity (m/s)	17, 26
Reynolds number (based on reference chord)	0.51×10^6, 0.78×10^6
Angle of attack, α (°)	-10 to 30 (step: 2)

4. Results and Discussions

The wind tunnel results for the experiment are divided into aerodynamic coefficients and pressure distributions above the wing. The first section of the results examined the correlation between aerodynamic coefficients with angle of attack at different Reynolds number. Figure 5 compares experimental data on lift, drag and pitching moment coefficients toward increasing angle of attack at different flow conditions. In general, all aerodynamic coefficients are slightly increased when Reynolds number change from Re = 0.51×10^6 to 0.78×10^6. From the lift coefficient data, a linear increment is observed from angle of attack -10° to 10° representing fully attached flow condition. As the angle of attack is increased, the lift curve become steeper and non-linear lift characteristics can be observed. The lift curved gradually increasing with rising angle of attack up to 26° before sudden lift loss indicating the wing stall. The observed increase in lift could be attributed to the formation of the leading-edge vortex above the wing. The drag production on the wing is surprisingly very low at 0° to 10° range. This contributes to higher lift-to-drag within angle of attack 5° to 10°. The highest lift-to-drag ratio recorded at α=8° indicating optimal cruise performance condition. It is apparent that the production of drag is higher at high angle of attack range (α>10°) due to lift-induced drag. Beyond 20°, severe drag production recorded due to vortex breakdown over the wing. For the pitching moment, there is slight distortion in the curve between $0° < \alpha < 5°$. Similar behaviour was found by Jentzsch et al. [21]. However, the exact cause for this nonlinearity is still not understood. The more pronounced nonlinear in pitching moment curved is observed at α >10° corresponding to the formation of strong leading-edge vortex at tip region of the wing. The dip trend in pitching moment curve at range of $16° \leq \alpha \leq 24°$ is due to the changes of the vortical flow topology above the wing.

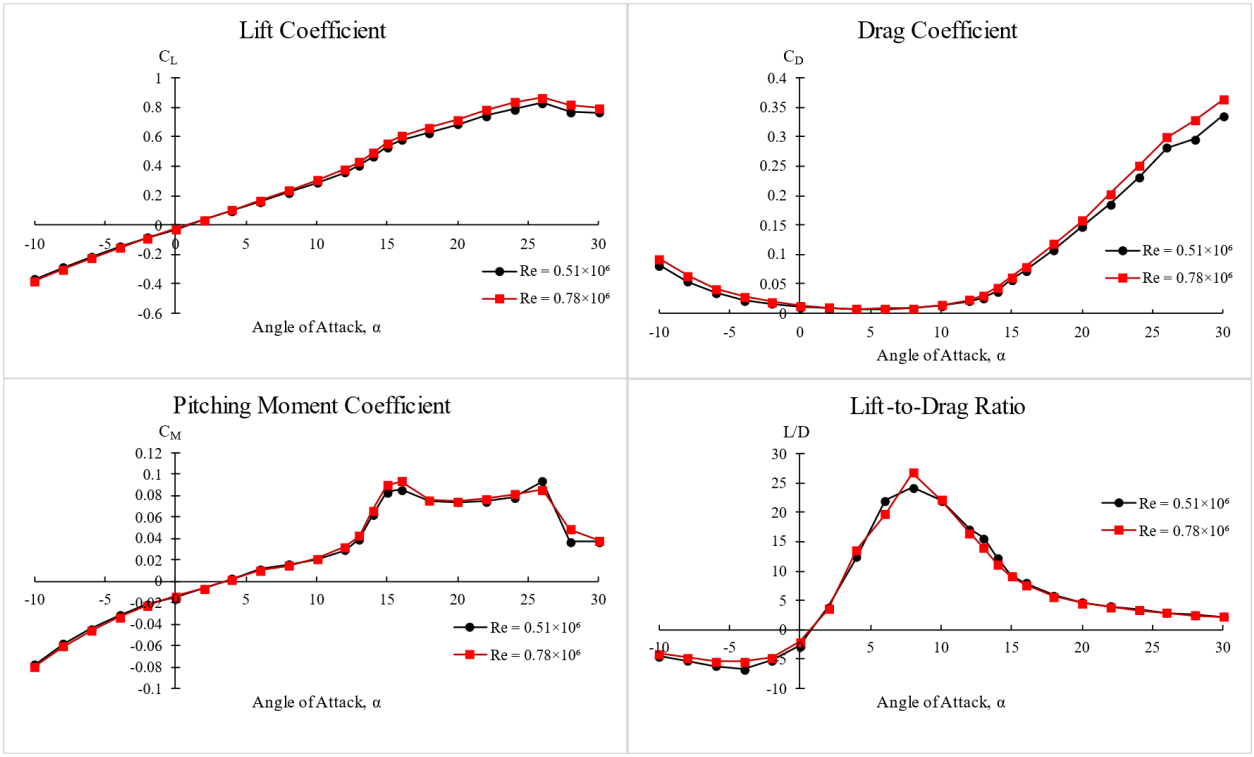

Figure. 5. Reynolds number effects on aerodynamic coefficients of UTM-SACCON

Figure 6 to Figure 8 represent the pressure distribution above the wing at angle of attack of 10°, 12°, 16°, 20° and 24°. In general, there are three distinct vortex structures above the wing namely based on the peak observed on the pressure distribution plots. The three vortex structures were named apex vortex, thickness vortex and tip vortex [16]. The tip vortex formation is having strongest suction based on the high peak trend on the pressure coefficient plot. At lower angle of attack (10°) it is observed that weak apex vortex developed in the region Y/Cr = 0.1 and 0.2. The formation of this vortex is due to sharp leading-edge profile in the apex region. However, this apex vortex only visible in the leading-edge region limited to front part of the model only. The characteristic of the vortex may partly be explained by the increase of wing thickness and increase in leading-edge radius downstream. Further downstream, the flow remained attached at the leading-edge region. At the Y/Cr = 0.4 inboard region, additional peak is observed indicating the other flow separation. The different in different profile between fuselage and wing section design produced uneven thickness distribution of the wing. The uneven elevation of the model top surface causing the flow to separate shedding a weak vortex. The aerodynamic coefficients observed however seems unaffected by the formation of both apex and thickness vortices. Downstream, the two vortices become weaker and diminished due to lower vorticity intensity. The tip vortex is observed to develop at angle of attack 12°. The formation of the tip vortex explained the changes in aerodynamic

coefficients by introducing additional lift on the wing. The onset separation of the tip vortex progressed upstream with increasing angle of attack. At angle of attack 16°, the progression of the tip vortex further upstream causing the thickness vortex to be drawn outboard near the vicinity of the tip vortex. This resulting in the merged between tip and thickness vortex forming larger and stronger outer vortex. The formation of the tip vortex justified the abrupt changed in pitching moment curved. One unanticipated finding was that downstream of the wing at Y/Cr = 0.9, another small suction peak was observable near the trailing edge region aside the tip vortex. This suction peak become more apparent at higher angle of attack α = 20° and 24° where the tip vortex already experienced vortex breakdown. The current finding is not reported from previous SACCON wind tunnel experiments and simulations which limited only at high Reynolds number of 1.6×10^6. The new suction peak may be resulted from the trailing edge shaped of the wing. The results obtained here has supported that another vortex is developed in the trailing edge region. Experimental pressure mapping is needed to verify this intensity flow.

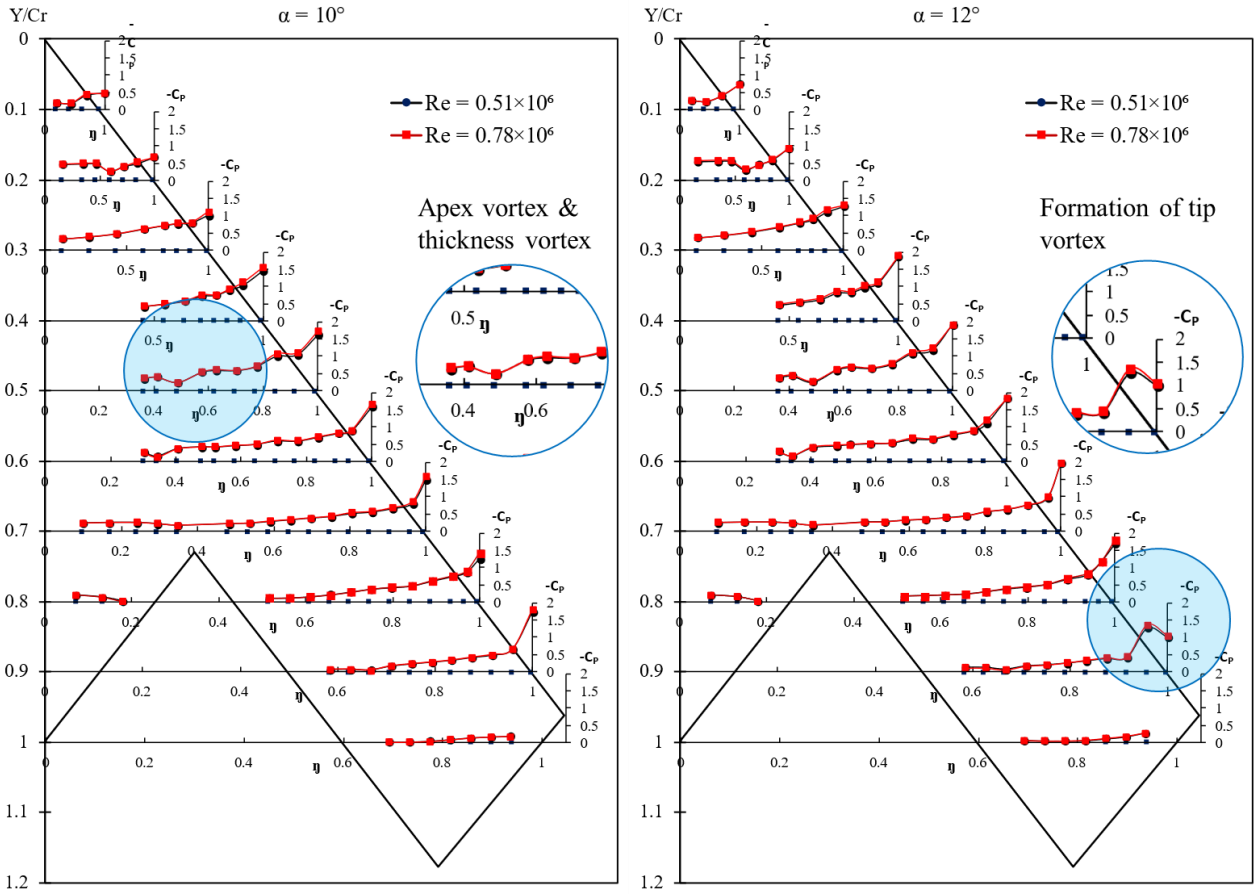

Figure. 6. Pressure distribution above the wing at angle of attack 10° and 12°

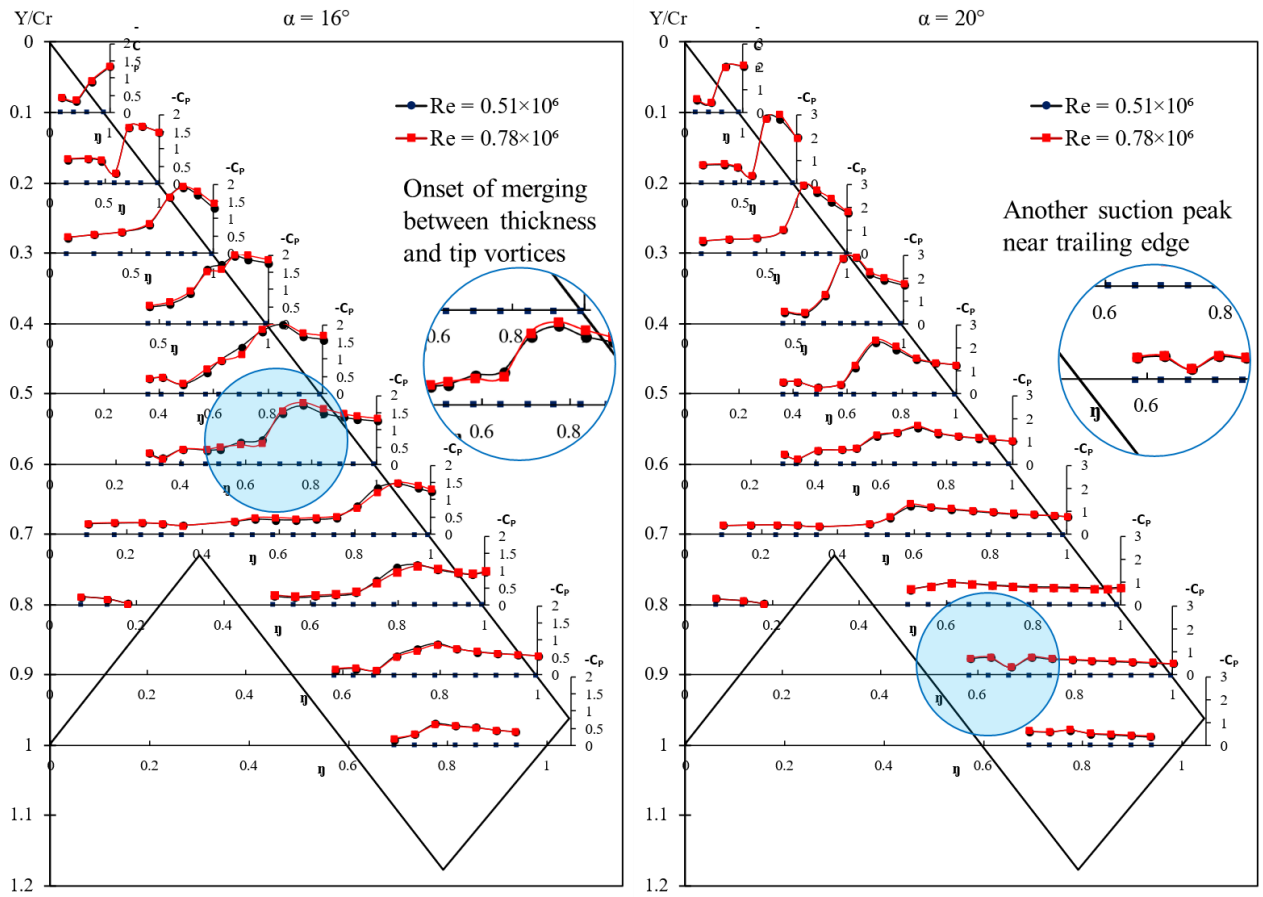

Figure. 7. Pressure distribution above the wing at angle of attack 16° and 20°

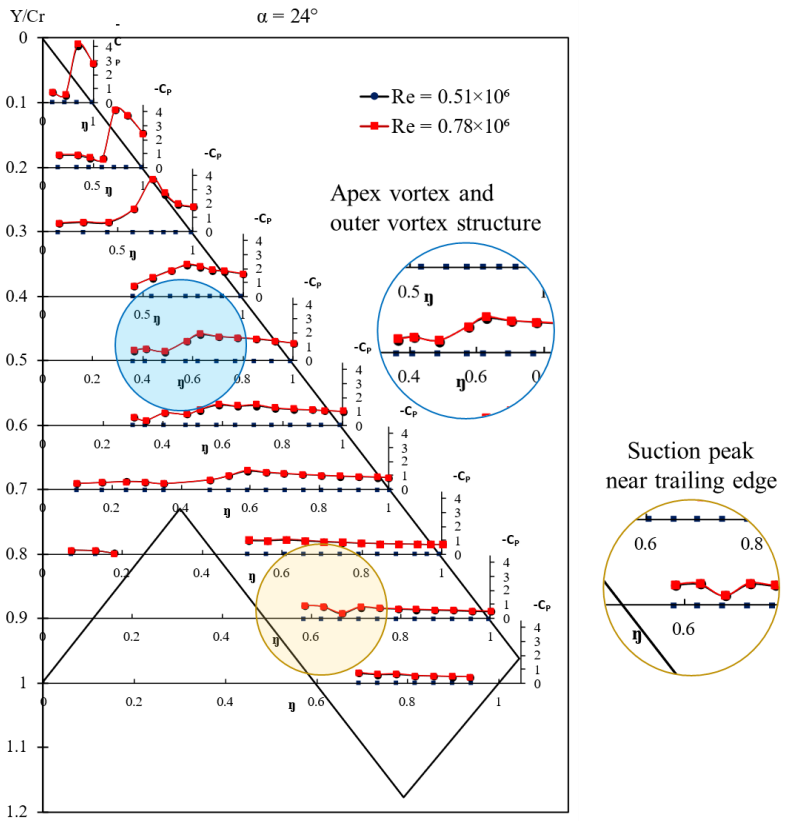

Figure. 8. Pressure distribution above the wing at angle of attack 24°

5. Conclusion

The flow structure above UCAV configuration is very complicated due to the interaction between different distinct vortex structures. The aim of the present research was to examine the effects of Reynolds number toward aerodynamic characteristic and on surface flow distribution of SACCON UCAV configuration. These findings suggest that in general the aerodynamic coefficients increased with increasing Reynolds number. The drag production on the wing is surprisingly very low at tested conditions resulting in high lift-to-drag ratio. The experimental data also conclude that the aerodynamic characteristics of SACCON wing is influenced by flow structure above the wing. The current experiment observed three different vortex structures developed on the wing namely apex vortex, thickness vortex and tip vortex at lower Reynolds number condition. One of the more significant findings to highlight from this study is that another suction peak developed on the wing suggesting new vortex structure above the wing.

Acknowledgment

This research was funded by the Universiti Teknologi Malaysia (Grant 21H05). The authors also would like to express their appreciation to the technical staff of the Universiti Teknologi Malaysia Aerolab (UTM Aerolab).

5. References

[1] Rogalski, T., Rzucidło, P., & Prusik, J. (2020). Unmanned aircraft automatic flight control algorithm in a spin maneuver. *Aircraft Engineering and Aerospace Technology*, 92(8), 1215-1224.

[2] Nawawi, S. W., Ahmed Abdou, A. A. M, & Abd Aziz, N. A. (2021). CNN-based Off-board Computation for Real-time Object Detection and Tracking Using a Drone. *Journal of Tomography System & Sensors Application*, 4(2), 11-20.

[3] Jusoh, M. I., Rosmin, N., Mustaamal, A. H., Aripriharta, Hussin, S. M., Amin, M. M., & Ali, N. A. (2021). A Review on Unmanned Aerial Vehicle for High Altitude Visual Inspection. *Journal of Tomography System & Sensors Application*, 4(2), 128-134.

[4] Li, Y. F., Shi, J. P., Jiang, W., Zhang, W. G., & Lyu, Y. X. (in press 2021). Autonomous maneuver decision-making for a UCAV in short-range aerial combat based on an MS-DDQN algorithm. *Defence Technology*, 1-18. https://doi.org/10.1016/j.dt.2021.09.014.

[5] Kováčik, L., & Novák, A. (2020). Comparison of Aerial Application vs. Ground Application. *Transportation Research Procedia*, 44, 264-270.

[6] Skjervold, E., & Hoelsreter, ϕ. T. (2018). Autonomous, Cooperative UAV Operations Using COTS Consumer Drones and Custom Ground Control Station. *MILCOM 2018 - 2018 IEEE Military Communications Conference (MILCOM)*, 29-31 October 2018, Los Angeles: IEEE.

[7] Chamola, V., Kotesh, P., Agarwal, A., Naren, Gupta, N., & Guizani, M. (2021). A Comprehensive Review of Unmanned Aerial Vehicle Attacks and Neutralization Techniques. *Ad Hoc Networks*, 111, 1-20.

[8] Gursul, I., Gordnier, R., & Visbal, M. (2005). Unsteady aerodynamics of nonslender delta wings. *Progress in Aerospace Sciences*, 41(7), 515-557.

[9] Gordnier, R. E., & Visbal, M. R. (2003). Higher-order compact difference scheme applied to the simulation of a low sweep delta wing flow. *41st Aerospace Sciences Meeting and Exhibit*, 6-9 January 2003, Reno: AIAA 2003-620.

[10] Schütte, A., Hummel, D., & Hitzel, S. M. (2012). Flow physics analyses of a generic unmanned combat aerial vehicle configuration. *Journal of Aircraft*, 49(6), 1638-1651.

[11] Maqsood, A., & Go, T.H. (2015). Aerodynamic characteristics of a flexible membrane micro air vehicle. *Aircraft Engineering and Aerospace Technology*, 87(1), 30-37.

[12] Tajuddin, N., Mat, S., & Said, M. (2020). Tomography Systems and Sensor Applications Flow Visualization Above Blunt-Edged Delta Wing. *Journal of Tomography System & Sensors Application*, 3(1), 86-97.

[13] Sepulveda, E., & Smith, H. (2017). Technology challenges of stealth unmanned combat aerial vehicles. *The Aeronautical Journal*, 121(1243), 1261-1295.

[14] Jordan, J. (2021). The future of unmanned combat aerial vehicles: An analysis using the Three Horizons framework. *Futures*, 134, 1-11.

[15] Liersch, C. M., Schutte, A., Siggel, M., & Dornwald, J. (2020). Design studies and multi-disciplinary assessment of agile and highly swept wing configurations. *CEAS Aeronautical Journal*, 11, 781-802.

[16] Nangia, R., Ghoreyshi, M., van Rooij, M. P. C., & Cummings, R. M. (2019). Aerodynamic design assessment and comparisons of the MULDICON UCAV concept. *Aerospace Science and Technology*, 93, 1-23.

[17] Cummings, R. M., & Schütte, A. (2010). An integrated computational/experimental approach to UCAV stability & control estimation: overview of NATO RTO AVT-161. *28th AIAA Applied Aerodynamics Conference*, 28 June - 1 July 2010, Chicago: AIAA 2010-4392

[18] Luckring, J. M., & Boelens, O. J. (2011). A unit-problem investigation of blunt leading-edge separation motivated by AVT-161 SACCON research. *Assessment of Stability and Control Prediction Methods for NATO Air and Sea Vehicles*. 27, 1-27, RTO-MP-AVT-189.

[19] Cummings, R. M., & Schütte, A. (2014). The NATO STO Task Group AVT-201 on 'Extended Assessment of Stability and Control Prediction Methods for NATO Air Vehicles'. *32nd AIAA Applied Aerodynamics Conference*, 16-20 June 2014, Atlanta: AIAA 2014-2000.

[20] Cummings, R. M., Liersch, C. M., & Schütte, A. (2018). Multi-Disciplinary Design and Performance Assessment of Effective, Agile NATO Air Vehicles. *2018 Applied Aerodynamics Conference*, 25 June 2018, Atlanta: AIAA 2018-2838.

[21] Jentzsch, M., Taubert, L., & Wygnanski, I. (2016). Active Flow Control on the Stability and Control Configuration (SACCON). *8th AIAA Flow Control Conference*, 13-17 June 2016, Washington: AIAA 2016-3168.